Impact of Ionospheric Anomalies on GBAS GAST D Service and Validation of Relevant ICAO SARPs Requirements

Sam Pullen*; Stanford University and Systems Enginuity, Inc.*
Rick Cassell*; Systems Enginuity, Inc.*
Bruce Johnson, Mats Brenner, Doug Weed, and Lucas Cypriano*; Honeywell*
Morten Topland and Morten Stakkeland*; Indra Navia (Norway)*
Boris Pervan*; Illinois Institute of Technology*
Matt Harris*; Boeing*
Susumu Saito*; ENRI (Japan)*
Jiyun Lee*; Tetra Tech AMT*
Barbara Clark and Shelly Beauchamp*; FAA*
Joseph Dennis*; Pragmatics, Inc.*

BIOGRAPHY

The International Civil Aviation Organization (ICAO) Navigation Systems Panel (NSP) has the responsibility of defining the international standards for Global Navigation Satellite Systems (GNSS). Within the NSP the Ground Based Augmentation System (GBAS) Working Group (GWG) is responsible for GBAS standards. The authors were part of a team within the GWG that performed the work described in this paper. The team and authors represent a diverse group of aircraft manufacturers, GBAS equipment manufacturers, aviation regulators, air navigation system service providers, academia and consultants.

ABSTRACT

The GAST D version of GBAS that supports Category II and III precision approach and landing operations adds additional monitoring to both the ground and airborne segments in order to minimize the differential errors that can be caused by anomalous ionospheric gradients. Extensive analysis and simulation work was conducted by a team within the International Civil Aviation Organization (ICAO) Navigation Systems Panel (NSP) to validate the performance requirements for ionospheric gradient mitigation. The analysis was specifically designed to confirm that the requirements could be met by the combination of ground and airborne monitors. This paper provides an overview of the validation activity. It includes a description of the design choices and monitors that make up the GBAS GAST D defense against anomalous ionospheric spatial gradients and the analysis and simulation results that demonstrate that the system successfully meets the performance requirements.

1.0 INTRODUCTION

Mitigation of ionospheric delays has been a challenging area for single frequency (GPS L1) Ground-based Augmentation System (GBAS) throughout its development. In the early 2000s, it was discovered that unusual ionospheric conditions over the Conterminous U.S. (CONUS) could create spatial gradients in slant ionospheric delay exceeding 400 mm/km, or over 100 times that observed during typical ionospheric behavior [1,2]. Anomalous ionospheric gradient observations from CONUS led to the construction of an ionospheric threat model that is generally applicable to mid-latitude regions [3]. Left unmitigated, these gradients can generate differential range errors that can translate into position errors of several meters or more for GBAS users. One implementation of a GBAS Approach Service Type (GAST) C service currently in operation to support Category I precision approaches mitigates this threat by detecting and excluding the vast majority of GPS satellites that if affected by anomalous gradients would contribute to unacceptably high position errors. It does this by performing "geometry screening" within the ground subsystem to inflate broadcast error parameters as needed to ensure that potentially unsafe satellite geometries cannot be applied by aircraft [4, 5]. Other mitigations of residual errors caused by anomalous ionosphere are possible. Solutions are workable, but can be cumbersome. Sometimes they result in a loss of availability

during nominal conditions if observability of local ionosphere conditions is not available or reliable. In such cases, conservative assumptions must replace real-time monitoring.

The GAST D version of GBAS is designed to support Category II and III precision approach and landing. The requirements are designed to meet the stringent performance needed for Category III autoland [6]. During validation of the ground subsystem Ionospheric Gradient Monitor (IGM) an unanticipated physical phenomenon was discovered, where relatively small-scale tropospheric delay gradients occur that appear to be caused by local atmospheric heating. It was found that these tropospheric delay gradients can cause false alerts in the IGM or possibly mask the detection of a hazardous ionospheric gradient. This issue prompted additional analysis, additional monitor requirements and further validation of the performance of the monitors.

Extensive analysis and simulation work was conducted by the team to validate the performance requirement for ionospheric gradient mitigation [7]. The analysis was specifically designed to confirm that the requirement could be met by the combination of ground and airborne monitors. GBAS ground subsystem manufacturers Honeywell International and Indra Navia developed simulations of GAST D aircraft approaches in order to quantify the effectiveness of the monitors in detecting gradients. A basic description of the modeling and simulation methods are contained in [8]. This paper provides an overview of the validation activity performed by the ICAO NSP GBAS Working Group that concluded in 2016. It includes a description of the design choices and monitors that make up the GBAS GAST D defense against anomalous ionospheric spatial gradients and the analysis and simulation results that demonstrated that the system successfully meets the performance requirements.

2.0 PERFORMANCE REQUIREMENTS

The existing SARPs (Standards and Recommended Practices) that support GBAS Category I (GAST C) operations are contained in ICAO Annex 10 [9]. The SARPs that support GAST D have been approved by the ICAO Navigation Systems Panel [10, 11], and will be formally published in 2018. The corresponding GBAS airborne Minimum Operational Performance Standards (MOPS) are contained in the recently published DO-253D [12]. In order to support Category III approach and landing the performance requirements for GBAS GAST D are the most demanding for aircraft navigation [13, 14]. The integrity requirements are defined to limit the failures that can cause erroneous guidance information to a probability of less than 10^{-9} per landing. The specific requirement allocated to anomalous ionospheric gradients limits the differentially corrected pseudorange error such that the probability of exceeding 2.75 meters at the Landing Threshold Point (LTP) is less than 10^{-9} per approach. The requirement allows for the prior probability of anomalous gradients to be considered in compliance. The LTP is located at the runway threshold. The rationale for the 2.75 meter value is to limit the magnitude of the error contribution of any one satellite to the navigation position solution. When translated into the position domain, this performance is sufficient to enable suitably equipped aircraft to meet the requirements for Category III autoland [15]. The ground manufacturer is responsible for ensuring that the combined air and ground monitors will not allow a maximum range error exceeding 2.75 meters at the LTP with a probability exceeding 10^{-9}, for any approach supporting GAST D. There are also requirements related to continuity. In the case of ranging source and ionospheric gradient monitors the continuity is allocated in terms of the probability of false exclusion of a satellite.

2.1 Threat Model

The validation assessment used the mid-latitude ionospheric threat model included in [9,10], which was extrapolated from the CONUS model in [3] to cover all known mid-latitude measurements with margin. The model is intended to represent a severe ionospheric spatial gradient as a moving wedge of constant, linear change in slant ionosphere delay, as shown in Figure 1. The key parameters of this model are the gradient slope (g) in mm/km, the width (w) of the wedge in km, the amplitude of the change in delay (D) in meters, and the speed (v) in m/sec at which the wedge moves relative to a fixed point on the ground. These values are assumed to remain (approximately) constant over the period in which this wedge affects the satellites tracked by a single aircraft completing a GAST D approach. Table 1 shows the threat model bounds on these parameters and on the gradient approach angles.

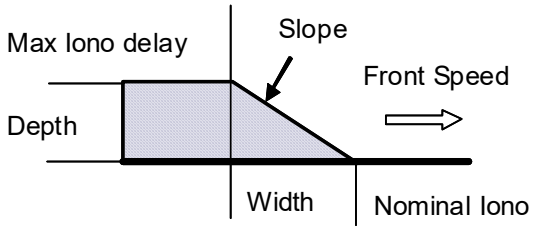

Figure 1. Moving Wedge Ionospheric Anomaly Model

Figure 2 illustrates the geometry for how ionospheric gradient scenarios are modelled. In all scenarios, the runway is in the north/south direction, and the aircraft approaches from the north. The gradient direction is indicated by the angle beta (β), where positive angles are to the east. The GBAS ground station reference receiver centroid is positioned at a maximum distance from the LTP, at an angle alpha (α), where positive angles are to the west. One of the mitigations to limit the impact of gradients is to restrict the distance between the GBAS ground station and the runway threshold below the 5 km that is typically assumed. The angles of the gradient and GBAS location are rotated to simulate all possible geometries.

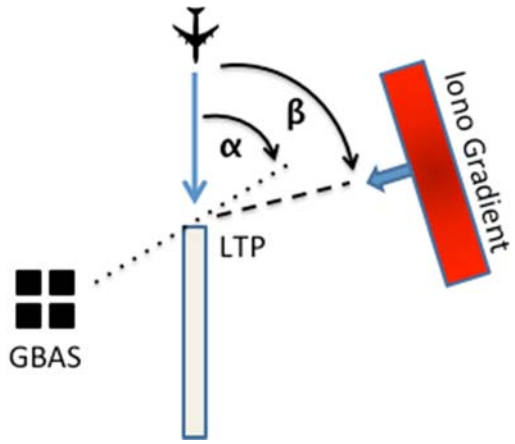

Figure 2. Ionospheric Gradient Scenario

Table 1. Gradient Threat Model and Direction Parameter Bounds

Parameter	Min	Max
Gradient Magnitude (g)	50 mm/km	500 mm/km
Max Delay (D)	N/A	50 m
Gradient Width (w)	25 km	200 km
Gradient Velocity (v)	-750 m/s	750 m/s
Gradient Direction β (wrt runway)	-90 degrees	90 degrees
GBAS Direction α (wrt runway)	90 degrees	270 degrees

The model scenarios also include defined aircraft ground speed profiles that are intended to be representative of a range of aircraft approach speeds [10]. Table 2 defines the parameters for the speed profiles. Evaluation of compliance is based on the combination of monitors meeting a probability of missed detection (P_{MD}) less than 10^{-9} for all scenarios with differential errors greater than 2.75 meters. The overall P_{MD} for multiple monitors is combined together taking into account the characteristics of auto- and cross-correlation on the monitor test statistics, as described in Section 4.2 [21].

Table 2. Aircraft Speed Profile from Start to LTP

Landing Ground Speed (knots)	Time at Landing Speed (seconds)	Deceleration Rate (knots/s)	Ground Speed Start of Deceleration (knots)
161	50	1.1	290
148	50	1.1	277
135	50	1.1	264

3.0 DESIGN MITIGATIONS

There are a number of changes implemented in GAST D that are intended to mitigate position errors due to ionospheric gradients, in order to meet the more stringent requirements for Category III autoland, without causing a degradation in availability. The navigation position solution uses 30-second smoothed measurements instead of the 100-second smoothing in GAST C to reduce the effective ionospheric divergence in the smoothing filter. The mitigation of ionospheric gradient threats in GAST D is a shared responsibility between the ground and airborne subsystems. The reason that the responsibility is shared is because each of the monitors can detect only a portion of the overall threat space, i.e. the threat may only be visible to the ground or airborne subsystem such that monitoring at both locations are required to mitigate the overall threat space. The ground subsystem IGM generates test statistics over reference receiver baselines to detect the observable impact of large spatial gradients (see [16, 17, 18]). The ground subsystem also includes a code-carrier-divergence (CCD) monitor, which aids in detecting a subset of ionospheric gradients. The design of the ground CCD monitor has not been defined in the standards, however one implementation used in the validation is described in 4.3.1.2.

There are also two airborne monitors that are part of the mitigation. The airborne subsystem also includes a CCD monitor, as well as a dual-solution pseudorange ionospheric gradient monitor (DSIGMA), which is based on the difference between 30-second and 100-second smoothed measurements in the range domain. The airborne CCD and DSIGMA monitors are designed to be capable of detecting ionospheric gradients that are observable to the aircraft, but not necessarily to the ground subsystem. There is also satellite geometry screening in the aircraft, which includes constraints necessary to limit the likelihood of large position errors that can occur, based on the aircraft performance needed to meet Category III autoland standards [6, 15].

3.1 Airborne DSIGMA Monitor

During the course of the validation of the mitigation of anomalous ionospheric gradients a new airborne monitor was developed, called the dual solution pseudorange ionospheric gradient monitor, abbreviated DSIGMA. This monitor computes the difference between the 30 second and 100 second corrected GPS pseudorange measurements as follows [12]:

$$P_{DIFF} = P_{corrected,\,100} - P_{corrected,\,30} \quad (1)$$

Where:

$P_{corrected,\,100}$ is the corrected pseudorange (meters), calculated using a carrier smoothing filter with a 100 second time constant.
$P_{corrected,\,30}$ is the corrected pseudorange (meters), calculated using a carrier smoothing filter with a 30 second time constant.

The validation of the DSIGMA monitor relied on flight tests conducted by both Honeywell under the Single European Skies Air Traffic Management Research (SESAR) program and by the FAA under their NextGen GAST-D validation project [19]. The flights only had nominal ionospheric gradients. Honeywell conducted data collection flights in June and July of 2014 and in July 2016 at locations including Frankfurt Airport (EDDF), Toulouse-Blagnac Airport (LFBO) and Atlantic City International Airport (KACY) for GAST-D validation. All of the ground stations used GAD-C multipath limiting antennas (MLAs) as reference antennas. All flights collected data using a Honeywell GAST-D prototype receiver with a 0.2 chip correlator and a dual-frequency Novatel receiver with a Pulse Aperture Correlator (PAC). The July 6, 2016 flight at KACY also used a Honeywell GAST-D prototype receiver with a 0.1 chip correlator.

The DSIGMA test statistic was calculated in post-processing to develop overbounding sigmas for different receiver correlator designs. Determination of the optimum threshold for the monitor involved balancing meeting the required integrity and continuity. The threshold was set based on the data illustrated in Figure 3, which was collected with a PAC correlator. It was determined that it is necessary to restrict the correlator spacing in the airborne receiver in order to meet the

defined performance. Testing of a 0.2 chip correlator resulted in noise and corresponding threshold that are too large to meet the derived detection performance. Therefore, it was decided to restrict the nominal correlator to 0.1 chips.

The analysis considered two approaches. The first approach would have a single threshold based on overbounding of all the data. The second case considered using two thresholds with separate overbounds based on elevation angle, with different threshold values above and below 30 degrees elevation. The analysis showed a small difference in the two approaches. This difference was not considered significant and the algorithm, as implemented, only has a single threshold. The overbounding sigma for the PAC data in Figure 3 was 0.131 meters. Conversion of this to a 0.1 correlator and including additional conservatism, the sigma overbound was adjusted to 0.174 meters. The allocated continuity for the monitor was $1x10^{-7}$. This was converted to a fault-free detection factor (K_{FFD}) of 5.61. Multiplying the sigma by this K factor results in a detection threshold of 0.976 meters.

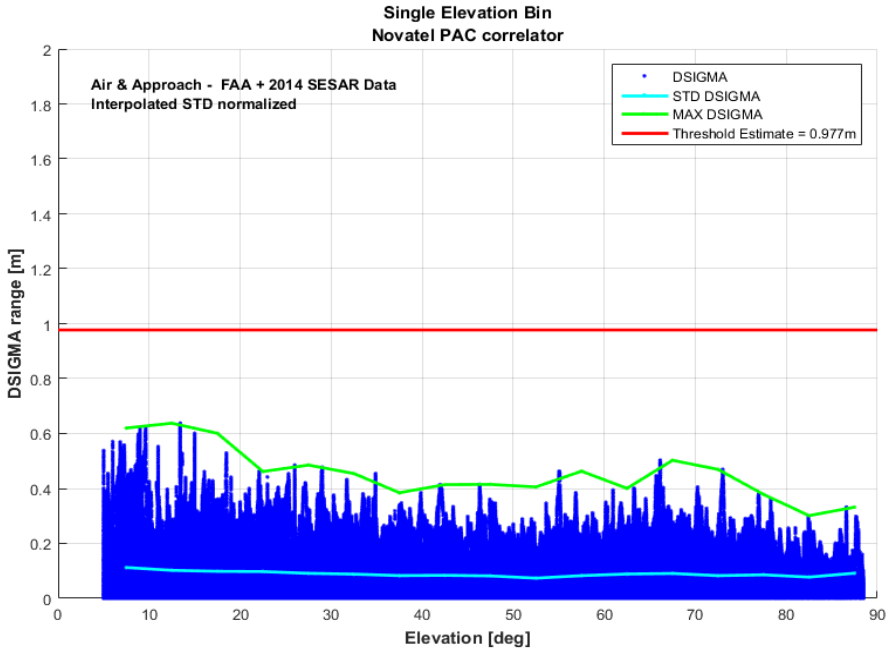

Figure 3. DSIGMA Monitor Test Results: Test Statistic vs. Elevation Angle

Testing and computer modeling determined that a newly risen satellite should not be added to the position solution unless P_{DIFF} has been computed for at least 200 seconds, when the aircraft is in the final approach region (10 NM from runway threshold). Because the concern for the impact is only on the final stages of Category III approaches, the DSIGMA monitor excludes satellites only within 3 NM of the runway threshold. The MOPS identifies four factors that are all required to occur simultaneously to exclude a satellite, and the satellite can be re-included when any of the four factors no longer exists: 1) a DSIGMA failure condition exists, 2) the computed ground speed is greater than 30 knots, 3) the computed position is less than 3 NM from the LTP, and 4) elapsed time since liftoff is greater than 5 minutes. The monitor is not required when the aircraft is taxiing since the GBAS is not providing surface guidance, other than during rollout. The monitor is not required when the aircraft is departing the airport since an ionospheric gradient, even if present, would not create a significant range error due to the proximity with the GBAS station. When operating near the ground, the receiver is subject to more ground multipath, which could lead to unnecessary monitor trips. Five minutes provides sufficient time to reduce the impact of ground multipath on the DSIGMA test statistic without permitting the introduction of significant error.

3.2 Airborne CCD Monitor

An airborne code-carrier divergence (CCD) monitor is required to operate at all times on each available ranging source for equipment supporting GAST D, while the use of the monitor outputs is limited to determination of ranging source suitability for the GAST D precision approach service. The airborne CCD monitor is a two-stage, or cascaded filter operating on the difference of the code-minus-carrier and is defined in the airborne equipment MOPS as follows [12]:

$$dz_n = \frac{[\rho_n - (\lambda/2\pi)\phi_n] - [\rho_{n-1} - (\lambda/2\pi)\phi_{n-1}]}{t_n - t_{n-1}} \quad (2)$$

$$Z_n = (1-k)Z_{n-1} + k \cdot dz_n \quad (3)$$

$$D_n = (1-k)D_{n-1} + k \cdot Z_n \quad (4)$$

where:

D_n is the filter output at epoch n,

Z_n is a filter state at epoch n,

k is the filter weighting function, a unitless parameter equal to the sample interval in seconds divided by a time constant of 100 seconds,

ρ_n is the raw pseudorange measurement in meters at epoch *n* (code loop carrier driven, 1st order or higher and with a one sided noise bandwidth greater than or equal to 0.125 Hz),

ϕ_n is the accumulated carrier phase measurement in radians at epoch *n*, and

λ is the carrier phase wavelength in meters.

The airborne CCD monitor is required to run at all times since the failure condition for this monitor is defined as a function of a history window, and a ranging source could be excluded from the GAST D solution if there is too much of the history window without computed filter outputs. The history window is defined as a window up to 20 minutes long, but not extending prior to 5 minutes after takeoff. Additionally, the full 20 minute history window can be avoided or restarted through vindication of the satellite using a fault detection algorithm that checks for consistency with the other non-faulted measurements.

A CCD failure is indicated for a satellite any time that the magnitude of the filter output ($|D_n|$), exceeds 0.0415 meters per second at any point in the CCD monitor history window or if more than 30 seconds of CCD outputs were not able to be computed in the history window. The satellite is then excluded from the GAST D solution within two seconds of the onset of all of the following conditions being met simultaneously:

a) A CCD failure condition exists; and
b) The elapsed time since liftoff is greater than 5 minutes; and
c) The computed ground speed is greater than 30 knots; and
d) The computed position is inside the final approach region.

The airborne CCD monitor is the first and most-effective monitor for detection of faster moving ionospheric anomalies that impact the airborne measurements prior to reaching the GBAS facility. The threshold was set to be as small as possible while still meeting an acceptable ranging source continuity level. The test statistic distributions for the monitor output were determined based on flight data from multiple aircraft and receiver types flown in Japan, United States, and Europe during quiet ionospheric conditions.

3.3 Ground IGM Performance

In May of 2014 the ICAO GWG was presented with evidence [20] that a tropospheric noise source was identified that could blind the Ionospheric Gradient Monitor (IGM) that was the core GBAS ground subsystem monitor proposed to mitigate ionospheric gradients. The IGM uses carrier phase double difference measurements between multiple satellites and multiple reference receivers. The tropospheric gradients that were observed were not sufficient to create large errors,

impacting integrity, but could blind the IGM to the presence of a hazardous ionospheric gradient or create a false trip of the IGM causing a satellite exclusion and impacting continuity.

A new strategy for ionospheric gradient mitigation was formulated using multiple monitors located both in the ground subsystem and airborne subsystem. A redesigned IGM was assigned the following performance requirements, in the presence of tropospheric gradient noise, to achieve the design Minimum Detectable Error (MDE) [21]:

$$K_{FD} * \text{continuity\_sigma} + K_{MD} * \text{integrity\_sigma} = \text{MDE} \quad (5)$$
$$5.54 * 16.7 \text{ mm/km} + 6.0 * 26.3 \text{ mm/km} = 250 \text{ mm/km}$$

Where:

$\boldsymbol{K_{FD}}$ **= 5.54** is the false detection factor derived from a probability of false detection (P_{FD}) system allocation of 3×10^{-8} in a 15 second exposure time, assuming 1 independent sample.

$\boldsymbol{K_{MD}}$ **= 6.0** is the missed detection factor derived from a probability of missed detection (P_{MD}) requirement within a 1.5 second time-to-alert of 1×10^{-9} for a 30 second exposure time.

Continuity_sigma = 16.7 mm/km is the maximum allowable overbounding sigma of the IGM gradient discriminator computed from all 4 Reference Receivers. The continuity sigma overbound is computed using an average continuity method, which uses all satellites over all days within the collected data set to compute the continuity sigma. The collected data set will be shown to be below this maximum continuity sigma value, providing design margin.

Integrity_sigma = 26.3 mm/km is the maximum allowable overbounding sigma of the IGM gradient discriminator computed from 3 Reference Receivers. The integrity sigma overbound is computed using the specific risk method where only the worst case satellite overbound sigma overbound over a single day from among all days within the collected data set is used. The integrity sigma overbound from the collected data will be shown to be below this maximum integrity sigma value, providing design margin.

A new Ionospheric Gradient Monitor (IGM) design approach was developed to reduce the effects of the tropospheric noise. Figure 4 and 5 show a comparison between the previous and new IGM methods for an active tropospheric day in Houston Texas from June 18, 2016. The weather conditions for this day were typical for severe tropospheric noise, with high temperatures (97° F) and humidity (74° F dew point), with scattered clouds and light winds. A comparison of the figures shows a reduction in the peak noise from over 250 mm/km for the previous IGM design to less than 75 mm/km for the new IGM design.

Using all visible satellites the continuity_sigma overbound was computed to be **15.1 mm/km** for the new IGM design compared to **61.8 mm/km** for the previous IGM design. The largest individual satellite integrity_sigma overbound was computed to be **21.3 mm/km** for the new IGM design compared to **89.9 mm/km** for the previous IGM design. Both of the new IGM design sigma's comply with the performance requirements listed above and result in the following MDE:

$$K_{FD} * \text{continuity\_sigma} + K_{MD} * \text{integrity\_sigma} = \text{MDE} \quad (6)$$
$$5.54 * 15.1 \text{ mm/km} + 6.0 * 21.3 \text{ mm/km} = 211 \text{ mm/km}$$

The computed MDE of 211 mm/km is 15% below 250 mm/km level which was used in ionospheric mitigation. This margin can account for more severe tropospheric noise as industry continues to evaluate this noise source.

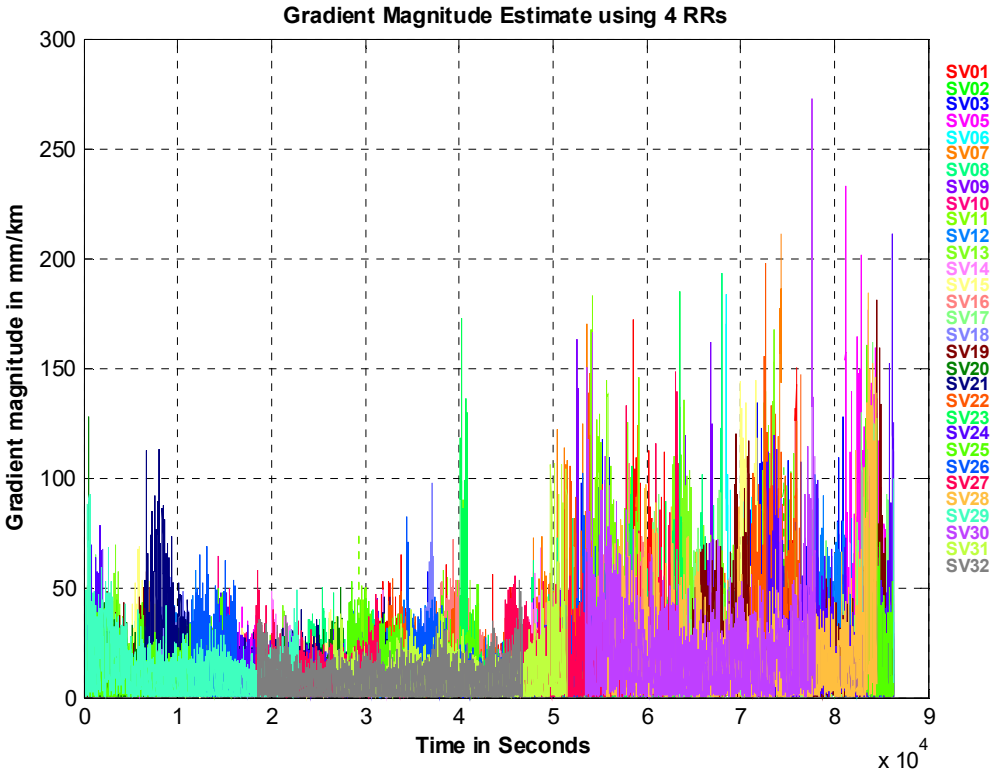

Figure 4. IGM Discriminators Computed Using Previous IGM Design

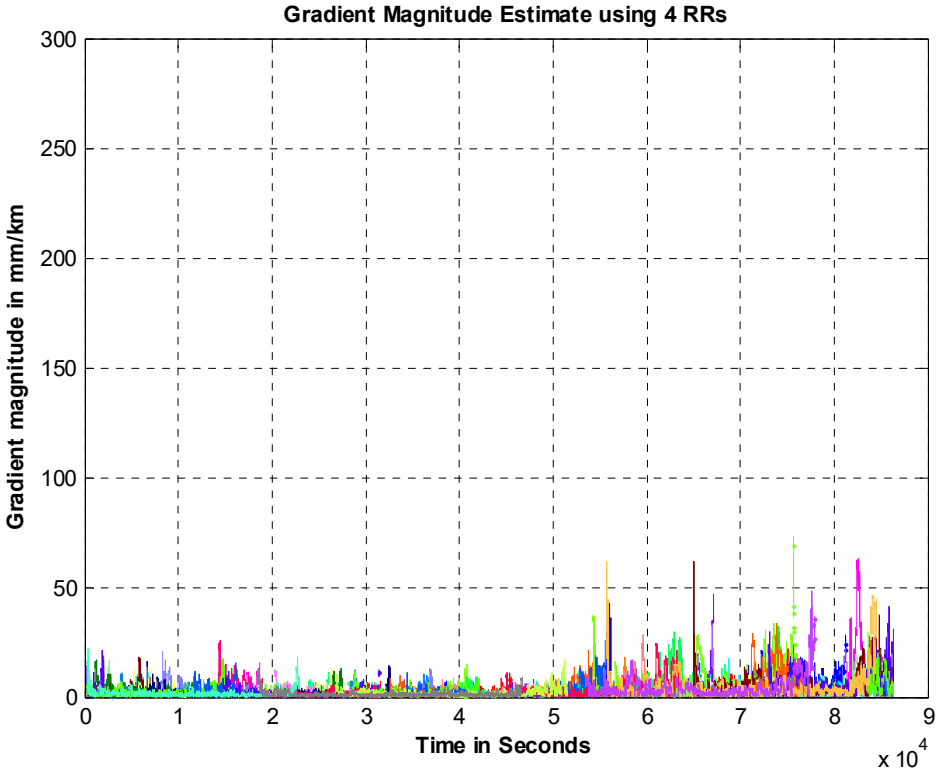

Figure 5. IGM Discriminators Computed Using New IGM Design

4.0 VALIDATION DESCRIPTION

4.1 General Approach

Because multiple GBAS ground and airborne monitors operate in the presence of anomalous ionospheric gradients of widely-varying behavior, simulations of these monitors in the presence of the anomalous gradient fronts described in Section 2.1 are required to fully analyze the threat that they pose [7]. These simulations execute the basic operations of GBAS ground and airborne subsystems, including the monitors described above, for a series of aircraft approaches in which each satellite out of the N in view at a particular time epoch is separately subjected to an ionospheric gradient with parameters chosen from the anomalous ionospheric threat model. How these parameters are chosen, and how the results of these simulations are combined, are key issues in determining if these results are sufficient for validation.

Two methods of selecting combinations of parameters are described below. The first is to discretize the ranges of variable parameters by step size so that the full range of possibilities is broken down into a finite set of discrete points. Each of these points is then exercised in the simulation for each time epoch and individual satellite impacted by an ionospheric gradient. As long as the discretization of the parameter space is sufficiently dense, this should determine which combinations generate the worst results (in terms of causing differential errors approaching or exceeding 2.75 meters with a P_{MD} approaching or exceeding 10^{-9}). The other approach is to use Monte Carlo simulation to sample from distributions of the variable parameters for each time epoch and affected satellite. This approach can be used as an alternative means of searching for worst case parameter combinations. Although the ICAO validation was not completed based on the Monte Carlo results, it was generally accepted that it could be used directly in an assessment of the requirement compliance if the asserted input parameter distributions are sufficient representations of factors that are random (unknowable) to the system and its users. Worst-case analysis (focused on finding and evaluating the very worst combinations of parameters) is described below in Section 4.3, while the use of Monte Carlo analysis is described in Section 4.4.

4.2 Monitor and Time Independence

This section addresses the influences of auto-correlation and cross-correlation of GBAS ionospheric monitor test statistics on the probabilities of false alert (P_{FA}) and missed detection (P_{MD}). In previous work, documented in [22], general analysis methods were derived to solve these problems. Here we summarize the most important analyses and results from that work relevant to GAST D validation, and documented in [23].

Cross-correlation between pairs of monitors directly influences the joint probability of missed detection, i.e., P_{MD}. Auto-correlation influences the probability of false alert, P_{FA}. Both probabilities, for DSIGMA, CCD-Ground, and CCD-Air monitors are heavily dependent on autocorrelation functions of raw code (pseudorange) multipath and noise and of nominal ionospheric spatial gradients and temporal divergence. The Boeing Company and the Thales Group provided, respectively, the necessary airborne and ground data to create autocorrelation models for multipath and receiver noise. Two nominal ionospheric spatial decorrelation models were used to represent both “low” (2mm/km) and “high” (4 mm/km) nominal vertical ionospheric gradients. All of the autocorrelation models used in the analysis are described in detail in [23].

Based on the DSIGMA and CCD-Air monitor P_{MD} results, it is safest to assume low-nominal ionospheric conditions, corresponding to scenarios where multipath and noise have increased influence. These are the blue curves in Figures 6 and 7. For the CCD-Ground monitor in Figure 8 there is only one nominal ionospheric model because spatial gradients are not relevant, so there is only one curve. The CCD-Ground monitor typically has a lower filter time constant (25 sec assumed) than CCD-Air (100 sec standard), and as shown in [23] the input multipath contributions also have lower time constants on the ground than in the air. For these reasons, the CCD-Ground monitor has more (effectively) independent samples during a 15 sec continuity interval. However, unlike DSIGMA, both of these monitors are heavily influenced by nominal ionospheric temporal divergence, which leads to an even larger number of independent samples for DSIGMA than for either of the other two monitors. For a typical normalized threshold $k_{FA} = 5.5$ and a 15 sec continuity interval, we can safely, and with margin, assume 5 independent samples for DSIGMA, 2 for CCD-Air, and 3 for CCD-Ground.

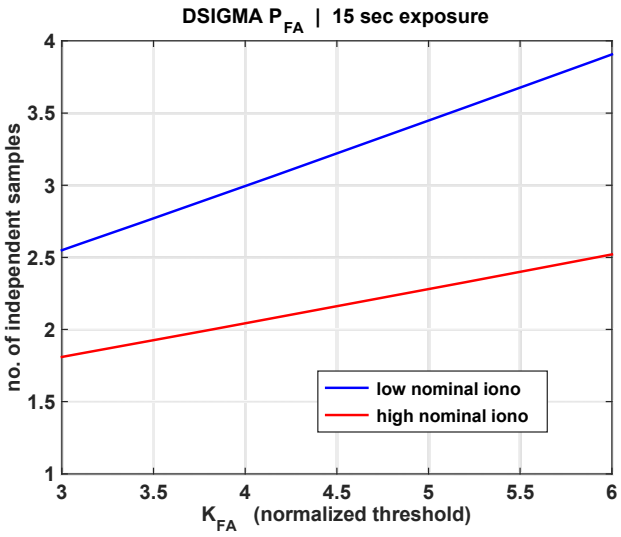

Figure 6. DSIGMA Monitor P_{FA} Independent Samples

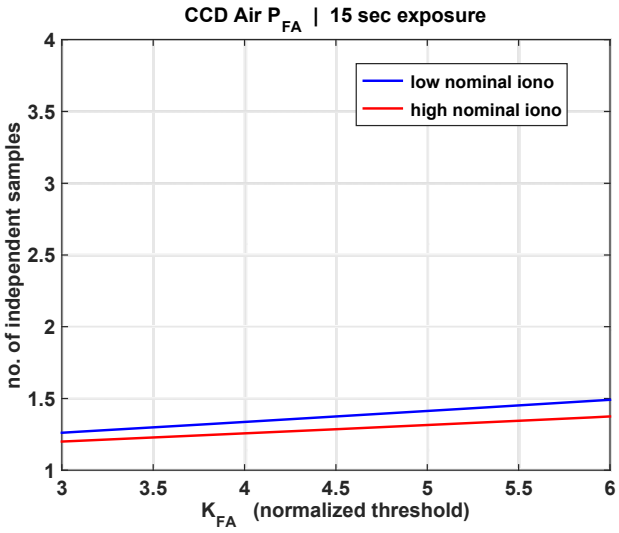

Figure 7. CCD-Air Monitor P_{FA} Independent Samples

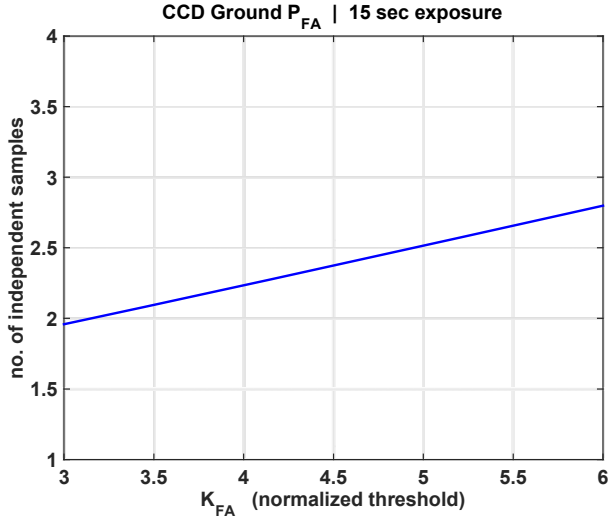

Figure 8. Effective Number of P_{FA} Independent Samples for CCD-Ground Monitor

The monitor cross-correlation results are shown in Figures 9 through 11. Figure 9 shows the cross-correlation impact between the CCD-Air and DSIGMA monitors. The CCD-Air monitor is dominated by nominal ionospheric temporal divergence, whereas the DSIGMA monitor is dominated mainly by multipath and noise. However, both monitors are additionally influenced by nominal ionospheric spatial gradients. For the low-level nominal gradient the monitors are essentially decorrelated, but at the high nominal gradient limit there is substantial correlation. Still, even in the latter case, an order of magnitude reduction in P_{MD} exists relative to either monitor alone, at least for integrity buffers with $k_{MD} \geq 3.5$.

Figure 10 shows the cross-correlation impact between the CCD-Ground and DSIGMA monitors. This case is the same as the previous one, except that the CCD-Ground monitor is not affected by nominal ionospheric gradients. The existence of a higher ionospheric gradient affects only the DSIGMA monitor in this case, causing even further decorrelation between the two monitors. The P_{MD} results in Figure 10 show that these two monitors are essentially independent. The correlation between the CCD-Ground and CCD-Air monitors is much more significant, because both monitors are heavily dominated by nominal ionospheric temporal divergence. The results in Figure 11 clearly indicate that P_{MD} credit can only be taken for one of these monitors.

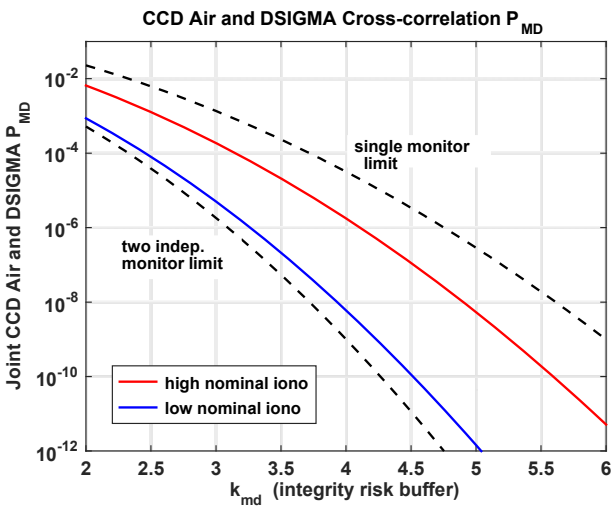

Figure 9. Joint P_{MD} for DSIGMA and CCD-Air

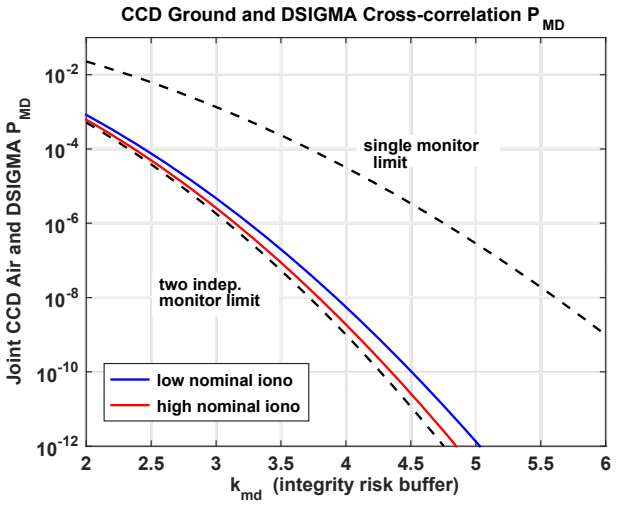

Figure 10. Joint P_{MD} for DSIGMA and CCD-Ground

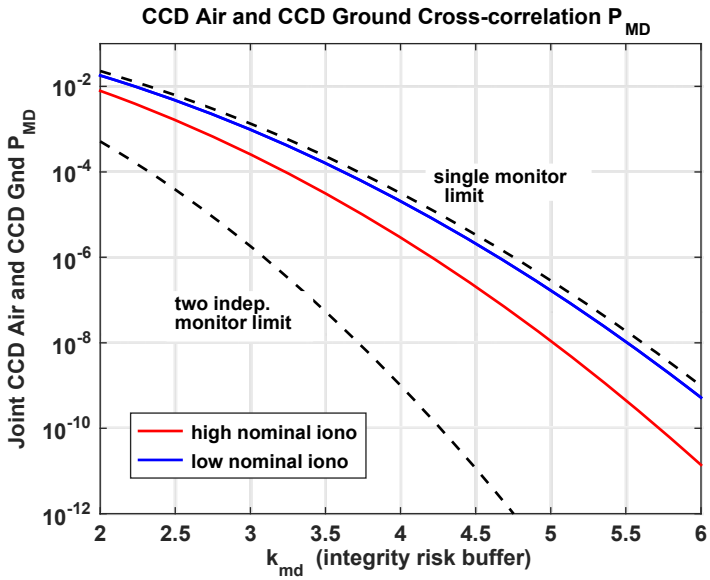

Figure 11. Joint P_{MD} for CCD-Air and CCD-Ground

Separate from the three monitors discussed above, GBAS reference stations will also use ground-based Ionospheric Gradient Monitors (IGM), as described in Section 3.3 and in [24] and [25]. These use input carrier phase measurements, so the multipath and noise errors affecting them will be essentially independent from those affecting the CCD-Air, CCD-Ground and DSIGMA monitors—because the multipath and noise in the latter monitors are dominated by code phase errors. In addition, nominal ionospheric spatial gradient effects on the IGM will be much smaller than at the aircraft, so we expect there will be negligible correlation with CCD-Air and DSIGMA test statistics. We also expect that CCD-Ground and IGM outputs will be essentially independent because the former is only sensitive to temporal divergence and the latter only to spatial decorrelation; and more importantly, as already noted, the CCD-Ground monitor it is most heavily influenced by code (not carrier) measurement errors. Nevertheless, a true understanding of IGM cross-correlation with other monitors, as well as its test statistic time correlation, requires knowledge and data available today only to ground system manufacturers, so final analysis for regulatory approval must be relegated to them.

4.3 Worst Case Analysis

4.3.1 Honeywell Results

This section describes the inputs, analysis and results that demonstrate validation of the SARPs ionospheric gradient requirements using a worst case validation method [26].

4.3.1.1 Analysis Methodology

The general approach used for Honeywell's worst case analysis is shown in Figure 12. Where the external input parameters are shown on the left, the simulation including three mitigating monitors are shown in the center and the performance results against the SARPs requirements are the output.

The external input parameters and SARPS requirements to compare the results against have been previously described in Section 2.0, as follows:

- Ionospheric Threat Space
- Set of 3 Airborne Speed Profiles
- Airport Geographic Parameters that include GBAS Reference Receiver centroid and ionospheric gradient location/motion as a function of orientation to the runway and aircraft approach path
- SARPS Ionospheric Integrity Risk Requirements

The validation simulation is noiseless. Therefore, all anticipated noise components of the airborne and ground monitor discriminators must be captured by overbounding the noise with a sigma value.

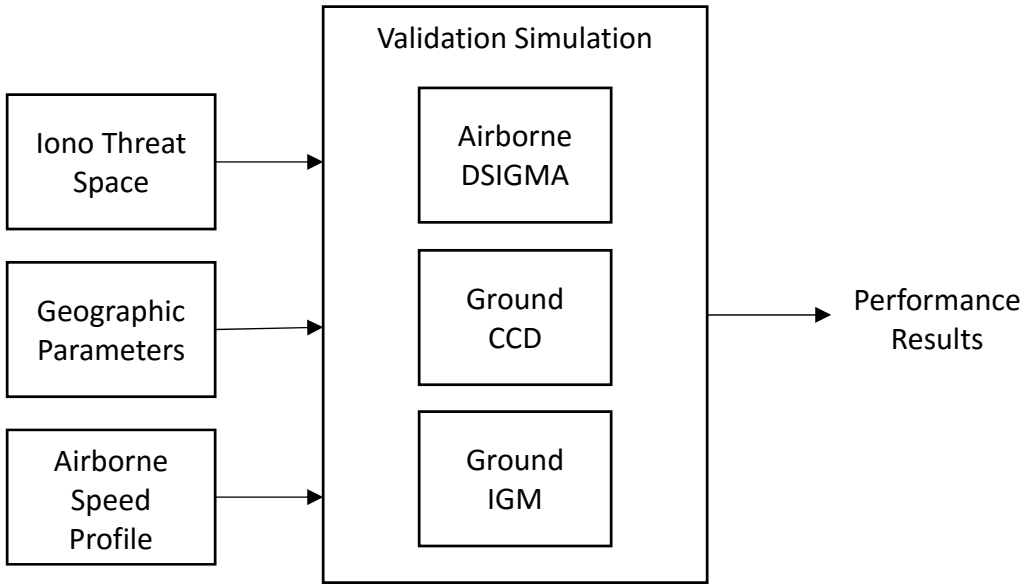

Figure 12. Honeywell Worst Case Validation Methodology

4.3.1.2 Input Combinations

The ionospheric threat space and geographic parameters are broken down to the parameter ranges and step sizes shown in Table 3. The validation simulation evaluates each combination of these parameters in combination with the three aircraft speed profiles in Table 2. Note that Table 3 is an extension of the threat model bounds in Table 1 and shows how that model is discretized into specific points that are simulated. In Table 3 the minimum gradient is shown as 200 mm/km instead of the actual minimum anomalous gradient of 50 mm/km from Table 1. This is because previous simulations have shown that gradients below 200 mm/km are never threatening to GAST D, as the maximum differential errors that they can produce are always below 2.75 meters.

Table 3. Honeywell Simulation Model Parameters

Parameter	Min	Max	Step Size
Gradient Magnitude	200 mm/km	500 mm/km	20 mm/km
Max Delay	N/A	50 m	N/A
Gradient Width	25 km	200 km	25 km
Gradient Velocity	-750 m/s	750 m/s	10 m/s
Gradient Direction β (wrt runway)	-90 degrees	90 degrees	15 degrees
GBAS Direction α (wrt runway)	90 degrees	270 degrees	15 degrees

The validation simulation incorporates three monitors, two ground based and one airborne, which collectively are expected to show SARPS ionospheric mitigation. Performance requirements for these monitors were defined as follows:

Airborne Subsystem Range Domain DSIGMA Monitor

The DSIGMA monitor is described in Section 3.1. Based on the DSIGMA monitor K_{FFD} of 5.61 and noise sigma of 0.174 meters taken from Section 3.1 and a K_{MD} of 6.0 (based on a missed detection probability of 1.0×10^{-9}) the minimum detectable error (MDE) for this monitor is computed as follows:

$$(K_{FFD} + K_{MD}) * \text{sigma} = \text{MDE} \quad (7)$$
$$(5.61 + 6.0) * 0.174 \text{ m} = 2.02 \text{ m}$$

Ground Subsystem Code Carrier Divergence (CCD) Monitor

The functionality of the ground CCD monitor was represented as two first order cascaded filters with time constants of 25 seconds and a discriminator noise sigma of 6.9 mm/sec. The resulting monitor threshold was 40.78 mm/sec based on an allocated false detection probability of 3.4×10^{-9} per monitor iteration (K_{FFD} = 5.91). The CCD integrity requirement is met with an allocation of probability of missed detection K_{MD} of 6.9. These values were proposed by Honeywell for GAST D validation. The resulting MDE for this monitor is computed as follows:

$$(K_{FFD} + K_{MD}) * \text{sigma} = \text{MDE} \quad (8)$$
$$(5.91 + 6.0) * 6.9 \text{ mm/sec} = 85.18 \text{ mm/sec}$$

Ground Subsystem Ionospheric Gradient Monitor (IGM)

This monitor was described in detail in Section 3.3, where the MDE was allocated to be 250 mm/km.

4.3.1.3 Validation Simulation

The validation simulation evaluates all combinations of the input parameters to confirm compliance with the SARPS requirement as described in Section 2.0. The SARPS performance requirement of 2.75 meters of differential range error is computed at a distance of 5 km from the ground subsystem reference receiver centroid to the LTP. This distance becomes a potential siting limitation for the ground subsystem. The total probability of miss-detecting the ionospheric gradient threat includes the prior probability of the ionospheric gradient and the combined airborne/ground monitoring probability of missed detection. For this validation effort, the prior probability of an ionospheric gradient threat was taken conservatively as 1.0.

The total required missed detection probability of 1.0×10^{-9} for any approach is provided by the combined probability of missed detection from all of the airborne and ground station monitors used in the mitigation case. It is assumed that the best (minimum) P_{MD} value for each monitor at any point in the simulation can be used. This is a conservative assumption as there generally will be multiple opportunities over the simulation time interval to detect the hazard. The simulation assumed that the discriminators from the ground CCD and the airborne DSIGMA monitors are correlated enough to not be considered independent. This assumption is conservative, as the analysis presented in Section 4.2 shows that they are essentially

independent. Therefore, the single best (minimum) P_{MD} from these two monitors was used and combined (multiplied) with the ground IGM P_{MD} to form the total P_{MD} used for validation.

4.3.1.4 Results

The ionospheric validation simulation was run to show compliance with the SARPS performance requirements described in Section 2.0. To accomplish this all hazards, accounting for the threat space, aircraft speed profiles and geographic parameters, with a range error of 2.75 meters must meet a probability of missed detection (P_{MD}) of 1.0×10^{-9}. The entire anomalous ionospheric gradient threat space is shown to be fully mitigated in Figure 13 assuming the ground subsystem CCD and IGM monitors meet the performance asserted in Section 4.3.1.2. Each dot in the figure represents a validation simulation run for a particular set of threat space, aircraft speed profile and geographic parameter conditions. The dot colors indicate the magnitude of the gradient, as shown on the right-hand vertical scale. Full mitigation is shown by not having any dots located in the upper right rectangle bounded by range errors larger than 2.75 meters and a missed detection probability greater than 1.0×10^{-9}.

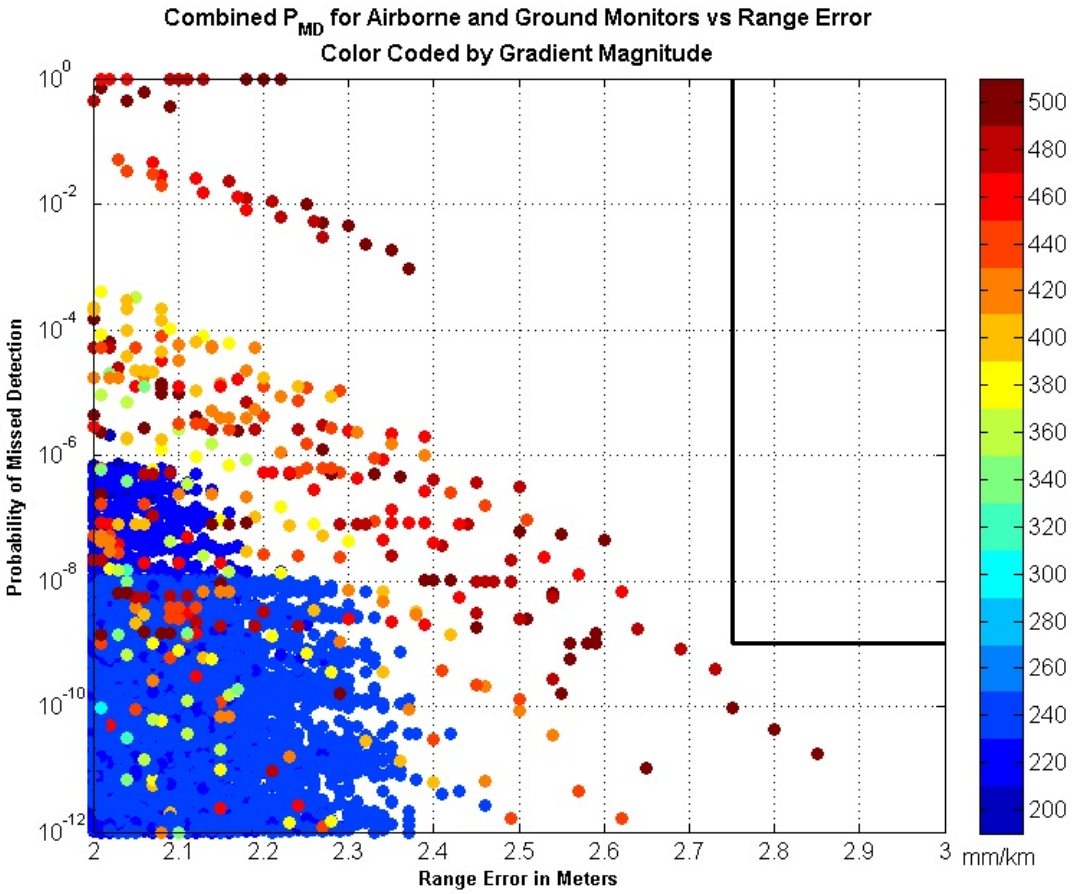

Figure 13. Honeywell P_{MD} vs Range Error for Ionospheric Gradient Sizes

4.3.2 Indra Navia Results

4.3.2.1 Simulation Inputs

The Indra Navia worst case simulations [27] use a method similar to that described for Honeywell (see Figure 6). Table 4 defines the range of values for the parameters included in the simulation model. Larger widths are omitted from the simulation since they do not produce noticeable effects on the results. The maximum ionospheric delay is set to 50 m, and the ground station centroid is located 5 km from the LTP. A convergence period of 360 seconds is assumed prior to broadcast of corrections from the ground station to let the smoothing filters converge, and the ground monitors are running during that

time. The value of 360 seconds is based on a requirement in EUROCAE ED-114A [28], although the requirement does allow a shorter time if the smoothing filters are sufficiently converged.

Table 4. Indra Navia Simulation Model Parameters

Parameter	Min	Max	Step Size
Gradient Magnitude	200 mm/km	500 mm/km	20 mm/km
Gradient Width	25 km	75 km	5 km
Gradient Velocity	0 m/s	250 m/s	10 m/s
Gradient Direction β (wrt runway)	-90 degrees	90 degrees	15 degrees
GBAS Direction α (wrt runway)	0 degrees	360 degrees	15 degrees

The simulation takes credit for a ground CCD monitor, an IGM and the airborne DSIGMA monitor. The ground CCD monitor uses two first order cascaded filters with time constants of 25 seconds, and a noise sigma of 4.3 mm/s is used for both continuity and integrity. Based on an allocated probability of false detection of $3x10^{-8}$, the detection threshold is 24.64 mm/s (K_{FFD} = 5.73). The performance of the IGM is assumed to be the same as described in Section 3.3, and the performance of the airborne DSIGMA monitor as defined in Section 3.1. The DSIGMA monitor is assumed to be running the last 50 seconds before arrival at the LTP. This is considered to be a rising satellite scenario where the satellite is visible for both the airborne user and the ground station the last 410 seconds of the approach. No credit was taken for the airborne CCD monitor. Credit is taken for the IGM being uncorrelated with the airborne DSIGMA and the ground CCD monitors, as described in Section 4.2.

4.3.2.2 Simulation Results

The resulting probability of missed detection from the worst case analysis performed by Indra Navia is presented in Figure 14 [29]. This result also shows compliance in meeting the required performance.

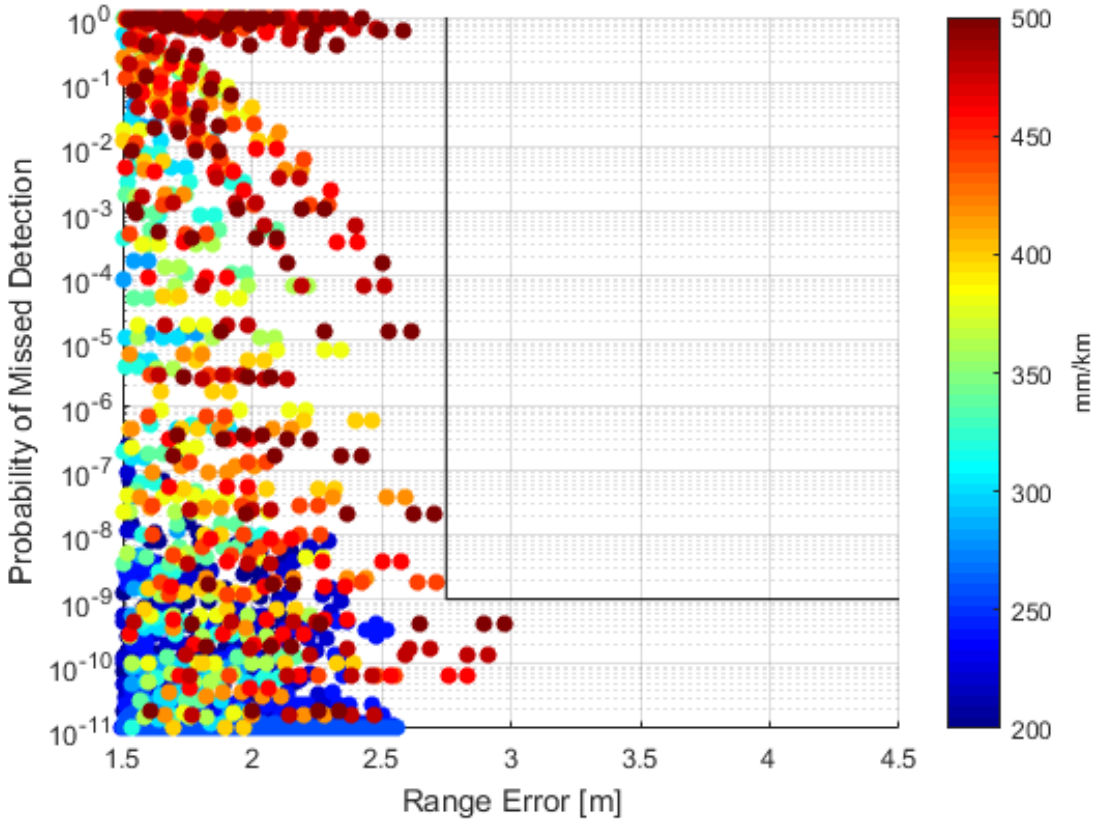

Figure 14. Indra Navia P_{MD} vs Range Error for Ionospheric Gradient Sizes

4.4 Monte Carlo Analysis

Assessment via simulation that uses Monte Carlo sampling to select threat model and aircraft approach parameters has been implemented by several organizations. The description that follows is the approach implemented by Honeywell as a variation on the worst-case methodology (based on discretization of the threat space) described in Section 4.2.1, and documented in [30, 31].

Figure 15 shows the structure of coding loops used to incorporate Monte Carlo sampling within the Honeywell simulation. Two outer loops simulate time epochs and sub-epochs at 5-minute and 15-second updates, respectively. Between these two loops is a loop of N_i samples of the relevant ionospheric front and aircraft approach parameters. Before these samples are conducted, two inner loops on the number of satellites in view at the user location chosen for this simulation and the aircraft approach angle to this location are executed. Note that these two loops ensure that each satellite and each aircraft approach direction are independently impacted by anomalous gradients.

For each iteration of these outer loops, an independent sample of the following parameters is drawn: LTP orientation (α), front width, front speed relative to the ground station, gradient magnitude, front direction (β), and aircraft position within the front when the approach threshold is reached. Each of these samples is taken from a uniform distribution with the minimum and maximum parameters shown in Table 3. These six sampled parameters are used together with the sampled aircraft approach angle and impacted satellite to conduct a single physical aircraft approach simulation in the presence of the sampled ionospheric gradient conditions. For Honeywell, this approach simulation is very similar to the one used in Section 4.3.1, and it applies each of the three ground and airborne monitors described in that section (also see Section 3). More details on this approach simulation are given in [8].

```
for Epoch [0, 288] (5-minute updates)
  for iteration [1, Ni] (1000 – 10,000 trials)
  for SubEpoch [1, 20] (15-second updates)
   for Nsat [1, numsat(subepoch)]
    for Approach Angle [–90, 90] in steps of 10 deg
      draw LTP Orientation (α) [–90, 90] deg
      draw width [25, 75] km
      draw front speed [0, 250] m/s
      draw gradient [200, 500] mm/km
      draw gradient front direction (β) [–180, 180] deg
      draw a/c position in front at threshold [0, width] km
        evaluate range error and vertical error for this trial
end loops
```

Figure 15. Loop Structure for Monte Carlo Sampling in Honeywell Simulation

At the end of each approach simulation, the aircraft's differential range error when the aircraft reaches the LTP is stored along with the combined missed detection probability (P_{MD}) of the GAST D ground and airborne monitors. The approach simulation includes zero measurement noise, thus the differential range error at the LTP due only to the ionospheric anomaly (based on 30-second steady-state carrier smoothing in both the ground and aircraft) can be observed directly at the end of each approach simulation. However, missed detection probabilities are different for each of the three monitors depending on when the sampled ionospheric front has its maximum impact on the ground station or aircraft. Given the thresholds and MDE values of each of these monitors from previous sections, P_{MD} values are computed for each monitor at each simulation epoch, and the minimum P_{MD} for each monitor over all simulation epochs when the monitor is active, leading up to the LTP, represents the P_{MD} contribution for that monitor. However, if a given monitor test statistic reaches a maximum value (and thus minimum P_{MD}) above its threshold (such that it would normally be excluded) but then falls back below the level (usually at 2σ) that would allow it to be readmitted into the position solution, the first minimum P_{MD} is not used, and the P_{MD} that is

used is the minimum value that occurs after this readmittance event takes place (see [8] for further details). In most cases, if the readmittance threshold is violated after exclusion, a delay in time is enforced before the affected satellite can be readmitted, meaning that the minimum P_{MD} corresponding to the original exclusion is retained until the delay expires and readmittance actually takes place (if this occurs before the approach ends). Next, based on the monitor cross-correlation analysis presented in Section 4.2, the individual monitor P_{MD}'s are combined into one overall P_{MD} as follows:

$$P(MD|\theta) = \min[(P(MD)_{\text{IGM}} \times P(MD)_{\text{DSIGMA}}), (P(MD)_{\text{IGM}} \times P(MD)_{\text{CCD}})] \quad (9)$$

where θ represents the vector of selected and sampled parameters from Figure 9 that were inputs to the approach simulation that produced these P_{MD} values. From this equation, one overall P_{MD} value results from each approach simulation and is paired with the differential error at the LTP that is also provided.

After all loops and samples have completed, the results of all N_{tot} scenarios, meaning the outcomes of each approach simulation triggered by each instance of the loops and samples shown in Figure 9, are combined to estimate the overall probability of Hazardously Misleading Information (HMI, representing an unsafe condition) as follows:

$$P(HMI) = P_{prior} \frac{1}{N_{tot}} \sum_{i \in \Psi} P(MD|\theta_i) \quad (10)$$

where P_{prior} represents the prior probability of the anomalous ionospheric events sampled in the Monte Carlo simulation of Figure 15 (here conservatively taken to be 1), and $i \in \psi$ represents the subset of all sampled events that have differential errors at the LTP that exceed a certain critical error value E, which is defined to be 2.75 meters by the GAST D requirements (see Section 2.0). Thus, Equation 10 sums the overall P_{MD} values (from equation 9) of all events in which the differential error at the LTP exceeds 2.75 meters, and this sum of probabilities is divided by the total number of sampled and simulated scenarios. If, for example, 10^7 scenarios were simulated, and of these, 10^3 scenarios had differential errors exceeding 2.75 meters with a mean P_{MD} of 10^{-9}, the resulting P(HMI) would be $(10^3)(10^{-9})/(10^7)$, or 10^{-13}. Note that scenarios with errors

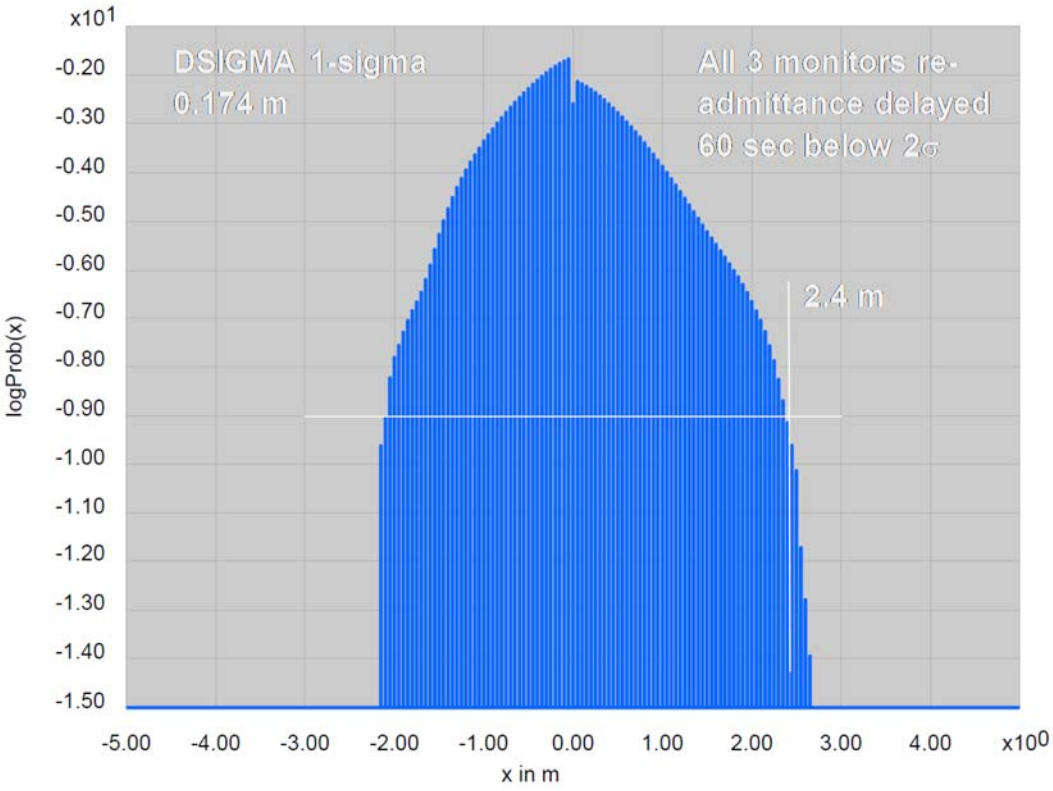

Figure 16. Histogram of Results from Honeywell Monte Carlo Simulation

below 2.75 meters are treated in the P(HMI) equation as having no safety risk at all, which is why the equation divides by all N_{tot} scenarios rather than some smaller number.

Figures 16, 17, and 18 show results obtained by Honeywell from this analysis technique using the monitor thresholds and MDEs from Section 4.3.1 with N_i = 5000 trials and a 60-second delay in measurement readmittance (if monitor test statistics for excluded measurements later fall below the 2σ readmittance thresholds). Figure 16 shows these results in the form of a histogram of samples of P(HMI) values on the *y*-axis (in log scale) versus differential error values on the *x*-axis, meaning that the error value *E* used to define the subset $i \in \psi$ in the P(HMI) equation was varied rather than being fixed at 2.75 meters. As a result, this plot shows that the required P(HMI) of 10^{-9} for GAST D is achieved at a lower error value of 2.4 meters, while P(HMI) at 2.75 meters is in the vicinity of 10^{-15} or lower. If the probability distributions assumed and number of samples taken can be justified and the averaging of risk shown in the P(HMI) equation above is accepted, then the GAST D requirement is met with margin.

Figure 17 shows a different view of the same simulation results. Here, differential errors are plotted versus the velocity of the sampled anomalous ionospheric front relative to the ground system for all scenarios with P_{MD} values at or above 10^{-9} (meaning those which are relatively hard to detect). Negative relative velocity for a particular scenario indicates that the ground system was impacted before the aircraft, whereas the reverse is true for positive relative velocity. While errors of 2.3 to 2.43 meters are seen at high positive and low negative relative velocities due primarily to the limits of IGM, errors that reach as high as 2.76 meters are shown for low positive relative velocities where the limitation of the airborne DSIGMA monitor plays the largest role. The red color of these points indicates that they are caused by gradients approaching the maximum of 500 mm/km allowed by the threat model, thus they greatly exceed the IGM MDE and should be reliably detected by IGM. However, the approach angle and relative phasing that applies to these particular scenarios weakens and delays the IGM response such that it is too late to reach full effectiveness (the aircraft reaches the LTP first).

Finally, Figure 18 shows these same results in the same format as Figures 13 and 14 for the Honeywell and Indra Navia worst-case simulations. Here, P_{MD} and differential range error are plotted against each other for scenarios where the P_{MD} is at or above 10^{-9}. Because this plot is based on sampled ionospheric parameters rather than looping through discrete points, the

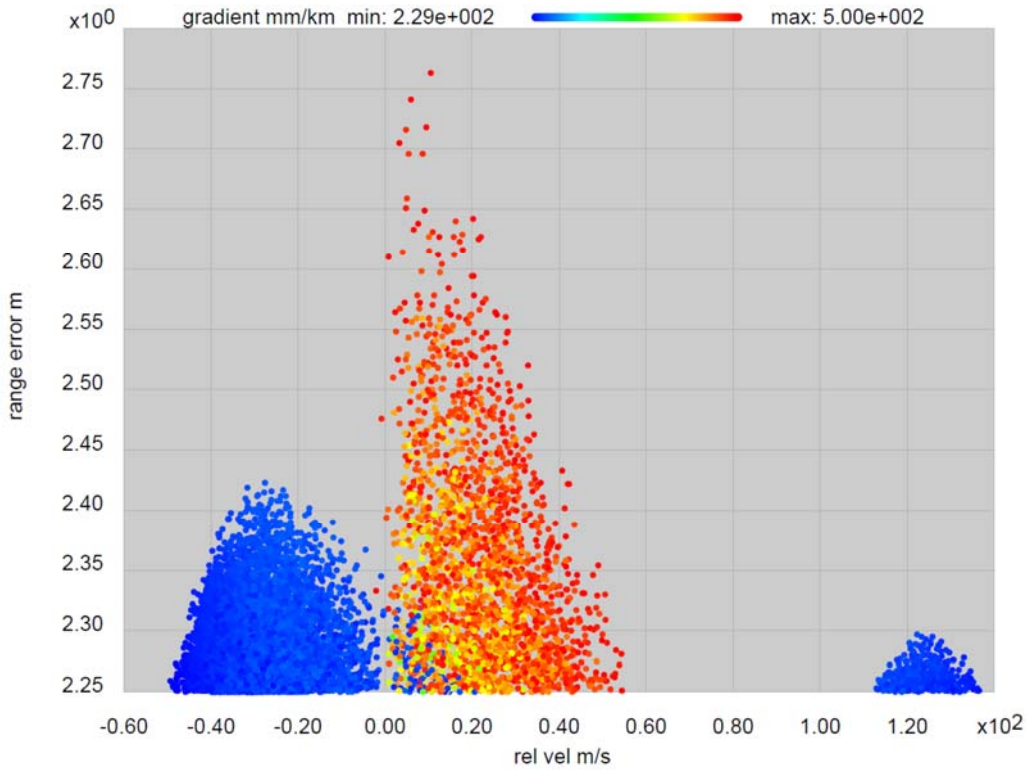

Figure 17. Differential Error vs. Front Relative Velocity from Honeywell Monte Carlo Simulation

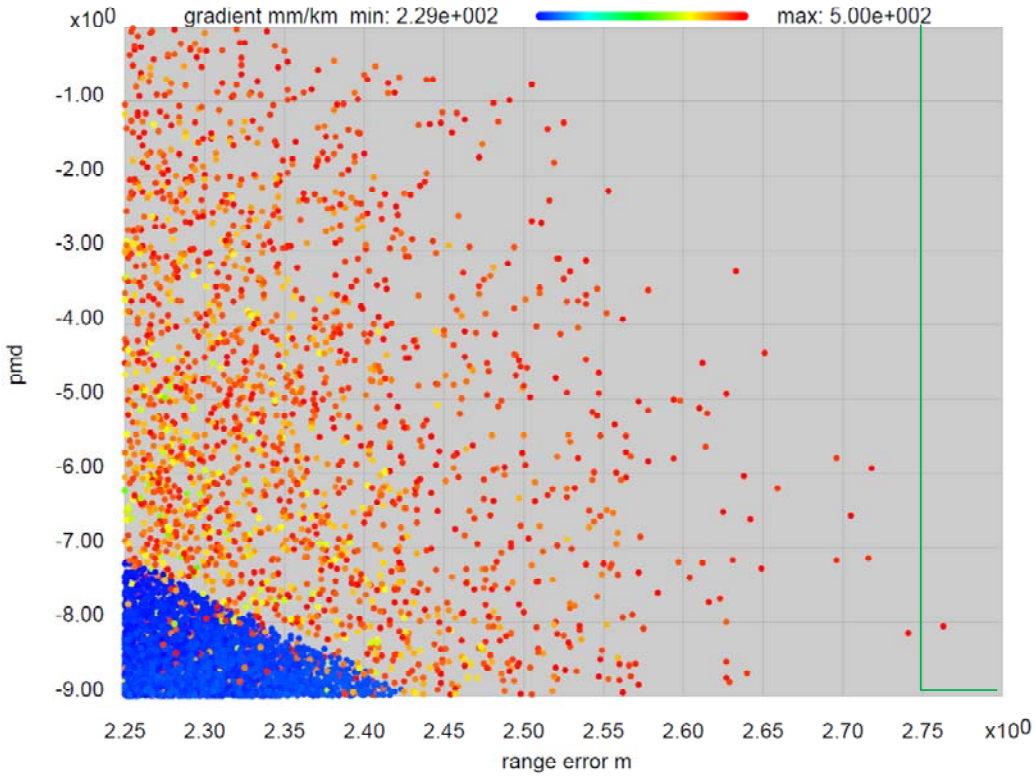

Figure 18. P_{MD} vs. Differential Range Error from Honeywell Monte Carlo Simulation

trends that appear in those earlier figures are less clear here, but the overall pattern is the same, in that the few points with errors approaching the 2.75 meter requirement have high gradients and relatively low P_{MD} values.

Because one point in Figure 18 just exceeds 2.75 meters with a P_{MD} of about 10^{-8}, it is believed that more-thorough sampling of the region of ionospheric, IGM, and aircraft approach parameters would reveal additional points that also exceed the GAST D requirements. This is not a problem for the Monte Carlo analysis method, since these few points are swallowed up by the many millions of less threatening points in the histogram of Figure 16. However, if they are a concern for the worst-case interpretation of the requirement, additional sampling in this region would be conducted to ensure that none of these points exceed the requirements by a significant amount or are part of a larger trend. Significance must be assessed given the fidelity of the modeling contained in the aircraft approach, satellite geometry, ionosphere, and GBAS monitoring simulations used in the analysis. Regardless, the results of the Monte Carlo analysis highlight the need for a thorough examination of the threat space to achieve an understanding of worst case undetected errors remaining after any given set of ionosphere gradient monitors.

5.0 SUMMARY

This paper has described the design characteristics intended to mitigate the impact of anomalous ionospheric gradients on the performance of GBAS GAST D to support Category II and III approach and landing. It has also described the methodology used to validate the specified requirements and the feasibility of achieving this performance. This included validation of the performance of the individual ground and airborne monitors designed to detect portions of the ionospheric gradient threat space.

The results this paper show that practically all of the worst-case ionospheric events within the mid-latitude threat model fall within the requirements of preventing range errors above 2.75 meters with missed-detection probabilities above 10^{-9}. The worst handful of events have gradients approaching the maximum of the threat model (500 mm/km) and slightly positive relative velocities that affect the aircraft before the ground system and delay both airborne and ground detection. The worst of these events, shown in Figure 18, has an error just exceeding 2.75 meters with a missed-detection probability of about 10^{-8}.

Such minor exceedances of the requirements are not a major concern and can be mitigated by small changes in ground monitoring or siting (e.g., reducing the separation between ground system and LTP below 5 km). However, it should be noted that little margin exists between the effects of the worst points in the mid-latitude threat model and the GAST D requirements. If probabilistic averaging is allowed to compute P(HMI), as described in Section 4.4 and shown in Figure 16, much more margin is present, as the few points that approach the boundaries of the requirements are a small subset of the threat space.

As described previously, the validation assessment is based upon the mid-latitude ionospheric threat model. More work is required to assess GAST D performance in low geomagnetic latitudes affected by plasma bubbles of depleted ionospheric delay. These bubbles are known to create larger maximum gradients than in mid-latitudes and smaller widths, meaning smaller distances between maximum and minimum delays [32, 33]. The ICAO GWG working group that completed the validation shown in this paper, along with other experts in low-latitude regions considering the use of GBAS (see [34]), are now investigating the effects of low-latitude ionospheric disturbances on GBAS.

REFERENCES

[1] A. Ene, D. Qiu, M. Luo, S. Pullen, P. Enge, "A Comprehensive Ionosphere Storm Data Analysis Method to Support LAAS Threat Model Development," *Proc. ION NTM 2005*, San Diego, CA, Jan. 24-26, 2005, pp. 110-130.

[2] J. Lee, S. Pullen, S. Datta-Barua, P. Enge, "Assessment of Ionosphere Spatial Decorrelation for Global Positioning System-Based Aircraft Landing Systems," *AIAA J. Aircraft*, Vol. 44, No. 5, Sept.-Oct. 2007, pp. 1662-1669.

[3] S. Datta-Barua, J. Lee, S. Pullen, M. Luo, *et al*, "Ionospheric Threat Parameterization for Local Area Global-Positioning-System-Based Aircraft Landing Systems," *AIAA J. Aircraft*, Vol. 47, No. 4, July-Aug. 2010, pp. 1141-1151.

[4] J. Lee, M. Luo, S. Pullen, Y. S. Park, P. Enge, M. Brenner, "Position-Domain Geometry Screening to Maximize LAAS Availability in the Presence of Ionosphere Anomalies" *Proc. ION GNSS 2006*, Fort Worth, TX, Sep. 26-29, 2006, pp 393-408.

[5] S. Ramakrishnan, "Targeted Ephemeris Decorrelation Parameter Inflation for Improved LAAS Availability During Severe Ionosphere Anomalies," *Proc. ION NTM 2008*, San Diego, CA, Jan. 28-30, 2008, pp. 354-366.

[6] "Conceptual Framework for the Proposal for GBAS to Support CAT III Operations," ICAO NSP/3, Montreal, Canada, Nov. 29 – Dec. 9, 2016, Flimsy 10.

[7] B. Johnson, ICAO Navigation Systems Panel, GWGs/1-WP2, "IGM Ad-Hoc Requirement Validation," Seattle, WA, 15-19 August 2016.

[8] D. Kim, M. Yoon, J. Lee, S. Pullen, D. Weed, "Monte Carlo Simulation for Impact of Anomalous Ionospheric Gradients on GAST-D GBAS," *Proc. ION Pacific PNT 2017 Conference*, Honolulu, HI, May 1-4, 2017, pp. 47-55.

[9] *Annex 10 to the Convention on International Civil Aviation: Aeronautical Telecommunications, Volume I Radio Navigation Aids*, Amendment 90, 10 November 2016.

[10] "Proposed amendments to Annex 10: Ground-Based Augmentation System (GBAS) provisions," ICAO NSP/3, WP-3, Montreal, Canada, Nov. 29 – Dec. 9, 2016.

[11] "GAST D SARPs Changes," ICAO NSP/3, Flimsy 6, Montreal, Canada, Nov. 29 – Dec. 9, 2016.

[12] "Minimum Operational Performance Standards for Local Area Augmentation System Airborne Equipment," DO-253D, RTCA, July 2017.

[13] T. Murphy, "Development of Signal in Space Performance Requirements for GBAS to Support CAT II/III Landing Operations," *Proc. ION GPS 2002*, Portland, OR, Sep. 24-27, 2002.

[14] C. Shively, "Treatment of Faulted Navigation Sensor Error When Assessing Risk of Unsafe Landing for CAT IIIB LAAS," *Proc. ION GNSS 2006*, Fort Worth, TX, Sep. 26-29, 2006.

[15] T. Murphy, M. Harris, C. Shively, L. Azoulai, M. Brenner, "Fault Monitoring for GBAS Airworthiness Assessments," *Navigation*, Vol. 59, No. 2, Summer 2012, pp. 145-161.

[16] S. Khanafseh, S. Pullen, J. Warburton, "Carrier Phase Ionospheric Gradient Ground Monitor for GBAS with Experimental Validation," *Navigation*, Vol. 59, No. 1, Spring 2012, pp. 51-60.

[17] J. Jing, S, Khanafseh, S. Langel, B. Pervan, "Detection and Isolation of Ionospheric Fronts for GBAS," *Proc. ION GNSS 2014*, Tampa, FL, Sept. 8-12, 2014, pp. 3526-3531.

[18] S. Saito, T. Yoshihara, S. Fujita, "Absolute Gradient Monitoring for GAST-D with a Single-frequency Carrier-phase Based and Code-aided Technique," *Proc. ION GNSS 2012*, Nashville, TN, Sept. 17-21, 2012, pp. 2184-2190.

[19] S. Beauchamp, S. Casler, L. Cypriano, M. Brenner, ICAO Navigation Systems Panel, GWGs/1-WP6, "Airborne DSIGMA Range Monitor Performance Validation Update," Seattle, WA, 15-19 August 2016.

[20] J. McDonald, D. Weed, B. Johnson, ICAO Navigation Systems Panel, WGW/WP16, "Observed Nominal Atmospheric Behavior Using Honeywell's GAST D Ionospheric Gradient Monitor," Montreal, Canada, 19-21 May, 2014.

[21] D. Weed, ICAO Navigation Systems Panel, GWGs/1-WP5, "Ground IGM Performance Validation," Seattle, WA, 15-19 August 2016.

[22] B. Pervan, S. Khanafseh, J. Patel, "Test Statistic Auto- and Cross-correlation Effects on Monitor False Alert and Missed Detection Probabilities," *Proc. ION ITM 2017*, Monterey, CA, Jan. 30 – Feb. 2, 2017, pp. 562-590.

[23] B. Pervan, ICAO Navigation Systems Panel, GWGs/1-WP7, "P_{FA}/P_{FD} Time Independence and Monitor Independence," Seattle, WA, 15-19 August 2016.

[24] R. Reuter, D. Weed, M. Brenner, "Ionosphere Gradient Detection for Cat III GBAS," *Proc. ION GNSS 2012*, Nashville, TN, Sept. 17-21, 2012, pp. 2175-2183.

[25] J, Jing, S. Khanafseh, S. Langel, F.-C. Chan, B. Pervan, "Optimal Antenna Topologies for Spatial Gradient Detection in Differential GNSS," *Radio Science*, Vol. 50, Issue 7, July 2015.

[26] R. Reuter, D. Weed, B. Johnson, ICAO Navigation Systems Panel, GWGs/1-WP3, "IGM Approach 2 Worst Case Validation," Seattle, WA, 15-19 August 2016.

[27] M. Topland and M. Stakkeland, ICAO Navigation Systems Panel, GWGs/1-WP4, "IGM Validation #2 Worst Case Method," Seattle, WA, 15-19 August 2016.

[28] "MOPS for Global Navigation Satellite Ground Based Augmentation System Ground Equipment to Support Category I Operations", ED-114A, EUROCAE, March 2013.

[29] S. Pullen, D. Weed, M. Brenner, M. Topland, ICAO Navigation Systems Panel, NSP/3-IP24, "Review and Reconciliation of Worst-Case and Monte-Carlo Ionospheric Anomaly Simulation Results", Montreal, Nov. 29 – Dec. 9, 2016.

[30] S. Pullen, M. Brenner, J. Lee, ICAO Navigation Systems Panel, GWGs/1-IP3, "Monte Carlo Simulation of Anomalous Ionospheric Impacts on GAST-D GBAS: Methodology and Input Probability Distributions," Seattle, WA, 15-19 August 2016.

[31] S. Pullen, M. Brenner, M. Stakkeland, ICAO Navigation Systems Panel, GWGs/1-IP1, "Updated Results of Monte Carlo Simulation of Anomalous Ionospheric Impacts on GAST-D GBAS," Seattle, WA, 15-19 August 2016.

[32] M. Yoon, J. Lee, S. Pullen, J. Gillespie, N. Mathur, R. Cole, J. Rodrigues de Souza, P. Doherty, R. Pradipta, "Equatorial Plasma Bubble Threat Parameterization to Support GBAS Operations in the Brazilian Region," *Navigation*, Vol. 64, No. 3, Fall 2017, pp. 309-321.

[33] S. Saito, S. Sunda, J. Lee, S. Pullen, S. Supriadi, T. Yoshihara, M. Terkildsen, F. Lecat, "Ionospheric delay gradient model for GBAS in the Asia-Pacific region," *GPS Solutions*, Vol. 21, Sept. 12, 2017, pp. 1937-1947. https://link.springer.com/content/pdf/10.1007%2Fs10291-017-0662-1.pdf

[34] T. Cashin, B. El-Arini, V. Massimini, R. Niles, A. Odeh, G. Zheng, S. Pullen, C. G. Wei, G. Shu, "Development and Implications of the Singapore GBAS Ionospheric Threat Model (GITM)," *Proc. ION GNSS+ 2017*, Portland, OR, Sept. 25-29, 2017.